Single Phase Mn_3O_4 Nanoparticles Obtained by Pulsed Laser Ablation in Liquid and Their Application in Rapid Removal of Trace Pentachlorophenol

Hemin Zhang, Changhao Liang,* Zhenfei Tian, Guozhong Wang, and Weiping Cai

Key Laboratory of Materials Physics and Anhui Key Laboratory of Nanomaterials and Nanotechnology, Institute of Solid State Physics, Hefei Institutes of Physical Science, Chinese Academy of Sciences, Hefei, 230031, China

Received: May 18, 2010; Revised Manuscript Received: June 16, 2010

We present a clean synthesis of well-crystallized pure Mn_3O_4 nanoparticles by pulsed laser ablation of an Mn metal plate immersed in deionized water at room temperature. The particle size, phase structure, and magnetic properties are characterized by X-ray diffraction, transmission electron microscopy, Fourier transform infrared spectra, and superconducting quantum interference device. The colloids solution of Mn_3O_4 nanocrystals with narrow particles size distribution could be facile obtained in a single step without addition of any other chemical reagents. As-synthesized pure manganese oxide nanoparticles show good performance in significant and rapid removal of trace amounts of pentachlorophenol. Thoroughly distinct from the general chemical process for growing manganese oxide nanoparticles, here the formation of manganese oxide nanocrystalline is based on reactions between laser-generated manganese species and water molecules in a local high-temperature and high-pressure plume−liquid interface region.

Introduction

Manganese oxides are important materials in many applications such as magnetic storage, catalysis, electrodes, ion exchangers, and sensors.[1−6] Among the series of manganese oxides, particularly, Mn_3O_4 is known to be an effective and inexpensive catalyst in various oxidation and reduction reactions; e.g., it can be used as a catalyst for the cracking of *n*-butane, isobutane, and propane[7] or the selective reduction of nitrobenzene to nitrosobenzene.[8] Moreover, Mn_3O_4 is an efficient, stable, and environmentally friendly catalytic material for the destruction of volatile organic compounds (VOCs)[9] and for the oxidation of hydrocarbon.[10] Mn_3O_4 has also been extended to sensing materials, such as gas sensors for actone,[11] a source of ferrite materials and manganese zinc ferrite,[12,13] and finding potential applications in electronics and information technologies. Nanoscale Mn_3O_4 with large specific surface area is expected to exhibit better performance in these fields of application.

Several synthetic methods have been developed to prepare nanoscale Mn_3O_4, such as the sol−gel process,[14] thermal decomposition,[15] and coprecipitation.[16] The sol−gel method has been found to be polluting, time-consuming, and expensive. The solvothermal method and sol−gel processes require posttreatment at different temperatures (>100 °C), and the thermal decomposition usually needs an atmosphere protection. In addition, preparation of single-phase manganese oxide nanostructures has always been a great challenge due to the multivalent states of manganese ions. We here report a clean and simple laser ablation approach to synthesize highly crystalline single-phase Mn_3O_4 nanocrystals. This approach requires neither sophisticated techniques nor any chemical reagent. Pulsed laser ablation in liquid (PLAL) has been widely used to prepare and modify the noble metal nanoparticles.[17−19] Interestingly, using an active main group or transition metal targets, pulsed laser induced reactive quenching in liquid medium, as a green (none pollution) method to prepare ultrafine nanoparticles, has recently been proven effective and flexible.[20−28] Strong reactions may take place between the ablated species and encountered solution molecules such as water since the most nascent ablation species of active metal targets are electronically excited and hence highly reactive. Thus, ultrafine metal oxide nanoparticles are expected to be obtained after rapid reactive quenching. The synthesized product is derived from its atomic constituents from the ablated solid and the participating liquid. To date, there have been no attempts reported about the PLAL method applied to the formation of manganese oxide nanoparticles. As one of the persistent toxic substances, pentachlorophenol (PCP) is carcinogenic and toxic to plants, animals, and humans even at low concentrations.[29] Adsorption is increasingly important to remove trace amounts of air and water pollutants, which adsorb very strongly on the adsorbent's surfaces. However, the regeneration of the adsorbent is one of the limitations of this process.[30] Ultrasound has been proven to be a very promising tool in overcoming the affinity between adsorbate and adsorbent and accelerating the molecular transport toward and from the adsorbent surface. Cavitation is responsible for this activation.[31] A series of compression and expansion cycles created by acoustic waves induced gas bubbles in the liquid to grow larger increasingly and eventually become unstable and implode, producing high-speed (approximately 400 km/h) microjets of liquid, intense localized heating, and high-pressure shock waves.[31] Manganese oxides are important material candidates for the removal of organic toxic pollutions via surface adsorption and oxidative degradation. We report the preliminary investigation of the removal of PCP using as-prepared Mn_3O_4 nanopartciles with fresh and clean surfaces and the effective desorption of PCP from Mn_3O_4 nanopartciles by ultrasonic treatment.

Experimental Details

Preparation of Mn_3O_4 Nanocrystals. The manganese metal plate with 99.8% purity was first fixed on a supporter in a vessel

* Corresponding author, chliang@issp.ac.cn.

10.1021/jp104510a
Published on Web 07/07/2010

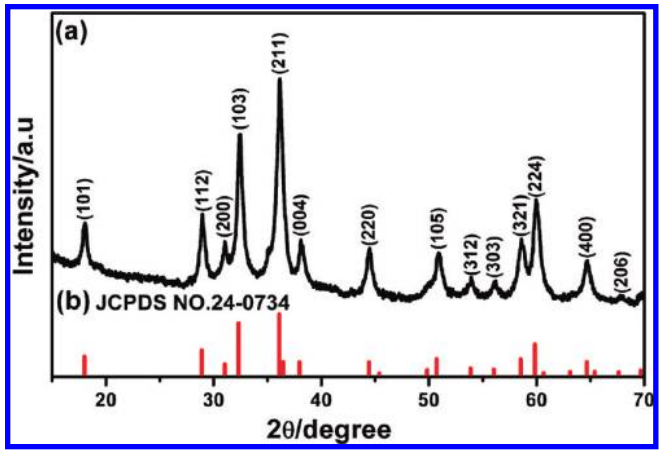

Figure 1. XRD pattern of (a) as-prepared Mn_3O_4 nanocrystals and (b) JCPDS Card No. 24-0734.

filled with 40 mL of deionized water. Then, the vessel was fixed on an automatic turntable, which was continuously rotated to avoid the damage by continuous ablation of laser pulses. The metal plate was irradiated for 30 min by the Nd:YAG laser with a pulse duration of 10 ns at 1064 nm wavelength and energy density of 80 mJ/pulse and spot size of 1.5 mm in diameter. After irradiation, the brown product was collected by centrifugation of suspension at 8000 rpm. The obtained powder products (productivity of about 0.33 mg/min) were ultrasonically dispersed with ethanol and then kept under vacuum in a drybox.

Characterization of Mn_3O_4 Nanocrystals. The X-ray diffraction analysis of the collected products was performed using a Philips X'Pert system with Cu Kα radiation (λ = 1.5419 Å, scanning rate 1.0°/min). The morphology and structure examination were conducted on a transmission electron microscope (TEM) (JEOL-2010) with 200 kV accelerated voltages. The specimen was made by dispersing the powder in ethanol to form a suspension and then dropping on a carbon-coated Cu grid. A Fourier transform infrared spectrum was taken on a NEXUS FTIR spectrometer. Magnetization measurements were carried out using a superconducting quantum interference device magnetometer (SQUID, Quantum Design MPMS) in the temperature range between 5 and 300 K. Acetic acid was used to adjust the pH value of the solution. The Mn_3O_4 nanoparticle powder was added to the solution in a sealed flask and placed on a shaker at room temperature. The content of PCP remaining in the solution was measured by an UV−vis spectrometer (Cary 5E UV−vis−NIR spectrophotometer) at 214 nm. The experiment of PCP desorption was carried out in an ultrasonic cleaner (JCX-400G, 20−100 kHz, adjustable output readings of 160−400 W).

Results and Discussion

Structure and Morphology. The X-ray diffraction (XRD) pattern of as-synthesized Mn_3O_4 nanocrystals is shown in Figure 1a. All diffraction peaks can be indexed to the tetragonal Mn_3O_4 structure (Figure 1b). The Mn_3O_4 lattice constants (a = 5.76 and c = 9.47 Å) obtained by refinement of the XRD data are consistent with the JCPDS database (No. 24-0734). The peaks of as-synthesized Mn_3O_4 nanocrystals were broader due to the smaller particle size. The calculation by the Debye−Sherrer formula gives an average particle size of 8.2 nm.

The morphology of Mn_3O_4 nanocrystals was observed by transmission electron microscopy (TEM). Low magnification TEM image of the as-synthesized nanocrystals is shown in Figure 2a. It can be seen that Mn_3O_4 nanocrystals were partially aggregated together. The size of aggregation was different from 15 to 30 nm. Figure 2b shows a typical HRTEM image of partly aggregated Mn_3O_4 nanocrystals. We can find that each aggregation was composed of several single crystals, which overlapped each other. Measurement of about 100 nanocrystals from more HRTEM images indicates that most nanocrystal sizes are from 7.1 to 9.2 nm (Figure 2c), which is concordant with the value obtained from the XRD measurement. The nanocrystals exhibited different crystal planes of tetragonal Mn_3O_4, such as (101), (112), and (200). From the inset image of Figure 2b, we observed that the marked lattice spacing coincided well with the (112) and (200) d-spacing, 0.309 and 0.289 nm, respectively, as reference to the JCPDS database (card No .27-0734) of Mn_3O_4. Selected area electron diffraction (SAED) analysis revealed that the nanocrystals were consistent with strong ring

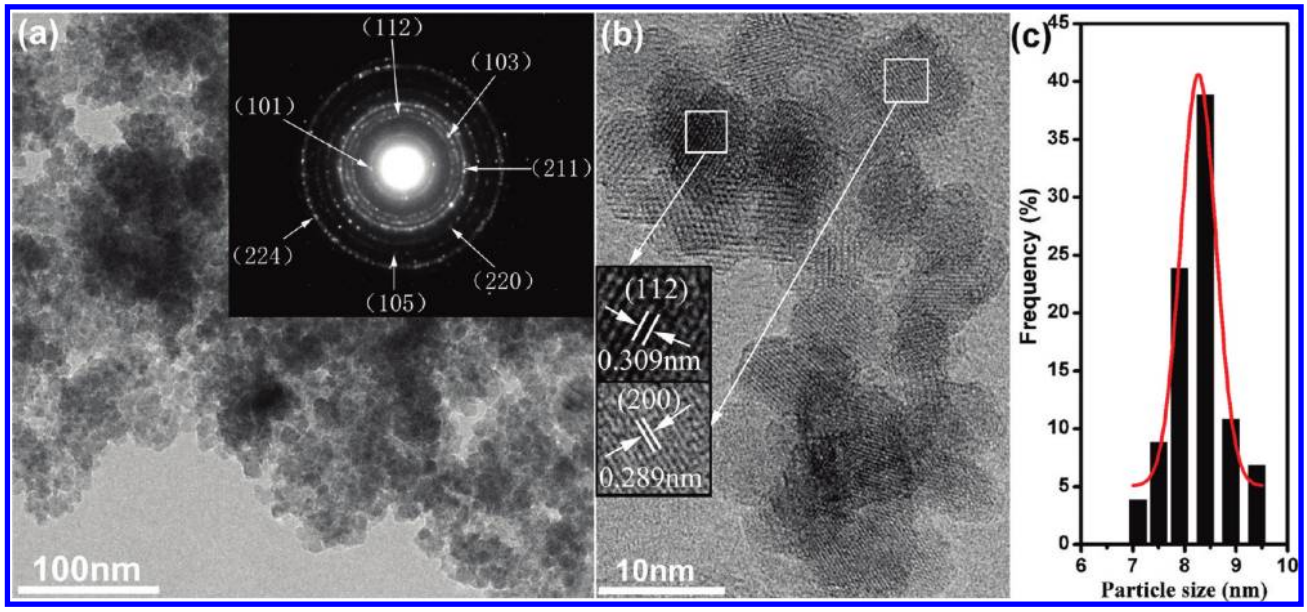

Figure 2. (a) Low-magnification TEM image and corresponding SAED pattern of Mn_3O_4 nanocrystals. (b) HRTEM lattice image of Mn_3O_4 nanocrystals. (c) Plotted particle size distribution of Mn_3O_4 nanocrystals.

SCHEME 1: Illustration of the Formation for Mn_3O_4 Nanocrystals by PLAL in Deionized Water

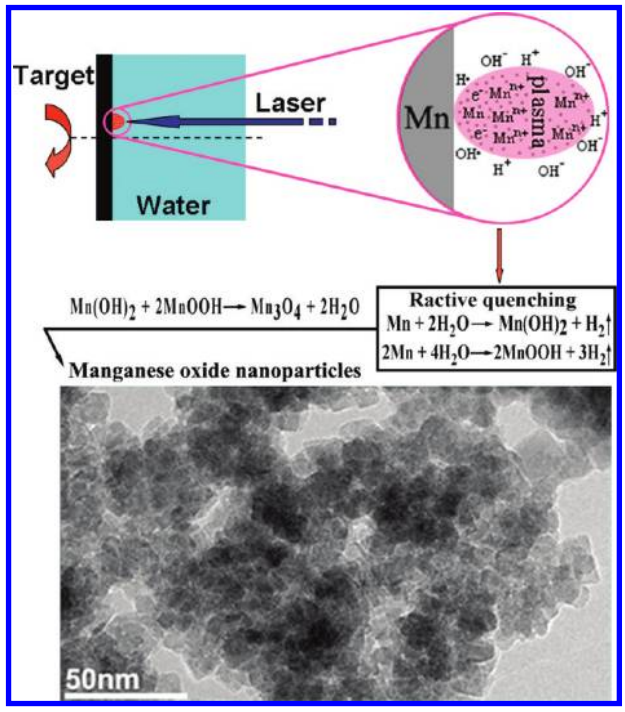

patterns due to (101), (112), (103), (211), (220), (105), (224) planes (inset of Figure 2a; see XRD pattern of Figure 1). A single highly crystalline nanocrystal of Mn_3O_4 should have regular shape according to XRD and HRTEM (regular TEM projection shape). Mn_3O_4 is known to have a spinel structure with a tetragonal distortion elongated along the *c* axis because of the Jahn−Teller distortion at the Mn^{3+} sites. The ionic formula of Mn_3O_4 can be written as $Mn^{2+}[Mn_2^{3+}]O_4$. In addition, octahedral nanocrystals can present rhomb, square, and circle shapes with projection along the crystalline axis of ⟨110⟩, ⟨001⟩, and ⟨111⟩, respectively.[33,34] Tetragonal nanocrystals can also be square and rectangle. Therefore, it is reasonable to observe different shapes of as-synthesized Mn_3O_4 nanocrystals upon HRTEM investigation (Figure 2b).

Formation Processes. Scheme 1 depicts the formation process of Mn_3O_4 nanocrystals. The PLAL generated manganese plasma plume containing electrons, manganese atoms, and diverse manganese ions will be formed at the solid−liquid interface rapidly after one pulsed laser irradiated manganese target.[35] Subsequently, the plasma plume with high temperature (about 6000 K) and high pressure (about 1 GPa) expanded adiabatically at ultrasonic speed. Simultaneously, the plasma plume vigorously reacted with water accompanied by rapid cooling in the plume−liquid interface region. This process may produce a large number of hydrogen radicals, hydroxyl groups, hydrogens, and hydroxide ions.[35,36] Finally, these ions and radicals that combined with manganese ions and atoms can grow into Mn_3O_4 under high temperature and high pressure. The checked pH value of solution changed from 6.5 to 8.6 after laser ablation, which may be attributed to the generation of hydroxyl ions. The process and chemical reactions can be briefly described as follows

$$Mn + 2H_2O \rightarrow Mn(OH)_2 + H_2\uparrow \quad (1)$$

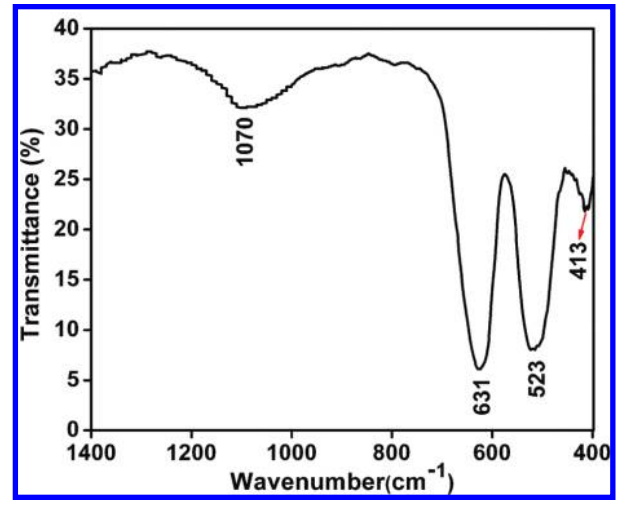

Figure 3. (a) FT-IR spectrum of Mn_3O_4 nanocrystals.

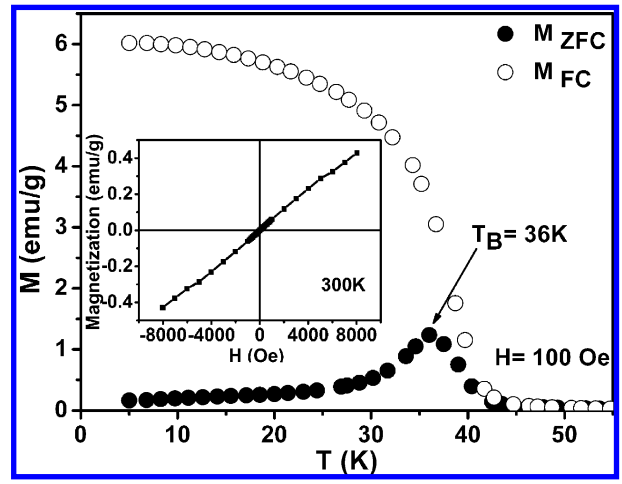

Figure 4. Zero-field-cooled (ZFC) and field-cooled (FC) magnetization curves of Mn_3O_4 nanocrystals under an applied field of 100 Oe. Inset shows magnetization curves at 300 K.

$$2Mn + 4H_2O \rightarrow 2MnOOH + 3H_2\uparrow \quad (2)$$

$$Mn(OH)_2 + 2MnOOH \rightarrow Mn_3O_4 + 2H_2O \quad (3)$$

FT-IR Analysis. The powders of Mn_3O_4 nanocrystals were analyzed by FT-IR spectroscopy. The spectrum (Figure 3) shows the characteristic absorption bands at 631, 523, and 413 cm^{-1}, which are assigned as the coupling modes between the Mn−O stretching modes of tetrahedral and octahedral sites, and the band at 1070 cm^{-1} can be attributed to ν(Mn−O−H) vibration.[37]

Magnetic Properties. Magnetic properties of the Mn_3O_4 nanocrystals were studied by using a superconducting quantum interference device (SQUID), shown in Figure 4. Bulk Mn_3O_4 (hausmannite) is ferromagnetic with a Curie temperature about 42 K. The as-synthesized Mn_3O_4 nanocrystals also show ferromagnetic property at low temperatures, whereas they are paramagnetic at room temperature (inset of Figure 4). Under zero-field-cooled (ZFC) measurements at 100 Oe, the blocking temperature T_B was 36 K. Under FC measurements with 100 Oe magnetic fields applied, the observed transition temperature was about 44 K. These results are well consistent with those reported by Park and co-workers for 6 nm Mn_3O_4 nanoparticles.[38]

Rapid Removal of PCP. Figure 5a shows that the absorption peaks of PCP at 214, 230, and 300 nm (pH = 3.0) rapidly

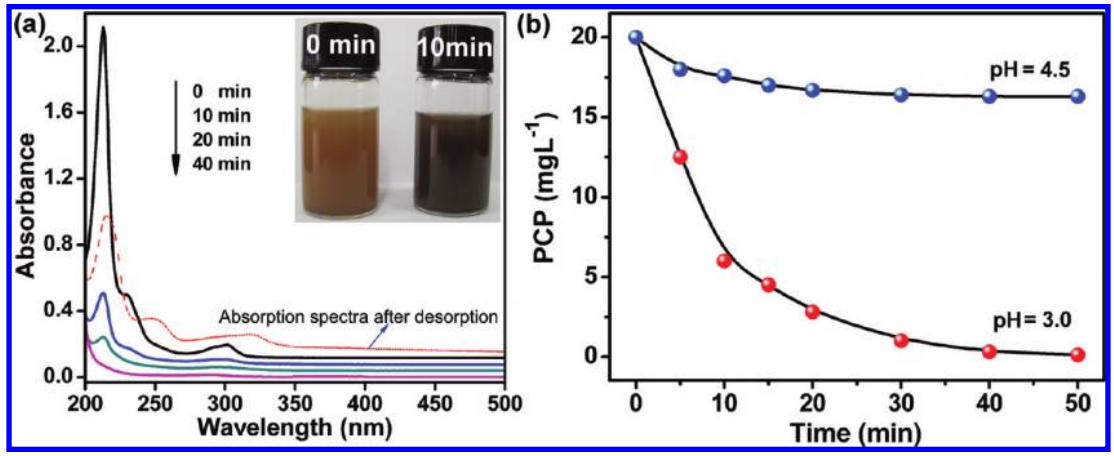

Figure 5. (a) UV−vis absorption spectra depicting the removal of PCP at pH = 3.0. (The dash line represents absorption spectra of ultrasonic desorption after 40 min contact.) (b) Time-dependent concentration change of PCP (starting concentration: 20 mg L^{-1}, 80 mL) in the presence of Mn_3O_4 nanoparticle powders (20 mg).

SCHEME 2: Schematic Illustration of pH-Dependent Absorption of PCP by Mn_3O_4 Nanoparticles

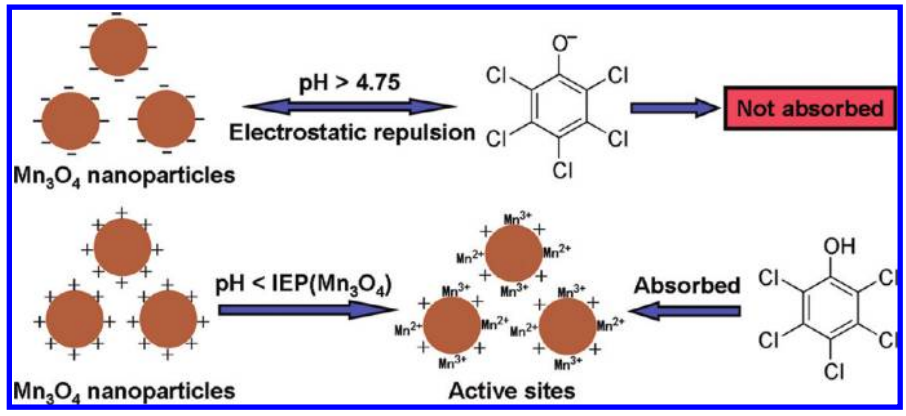

decrease in intensity with the contact time and almost disappear after 40 min. When the pH value of the solution was approximately 3.3−5.2, the removal rate of PCP became very low (Figure 5b, pH = 4.5). Figure 5b (pH = 3.0) shows the related plot between the contact time and the concentration of the residual PCP. When the contact time reaches 10 min, about 75% PCP can be removed and the color of Mn_3O_4 solution changed from brown to black caused by the formation of precursor complex (inset of Figure 5a). When the contact time is sustained for 40 min, almost 98.5% of the PCP can be removed. It is thought that the surface charging states of nanoparticles play critical roles in the removal of PCP. When the pH value of solution was larger than the isoelectric points (IEPs) of Mn_3O_4, the surfaces of Mn_3O_4 nanoparticles were negatively charged, otherwise the surfaces were positively charged. When the pH value of solution exceeded 4.75 ($pK_a = 4.75$,[39] mostly existing in an ionized form due to deprotonation), the surfaces of most PCP molecules were negatively charged, whereas the surfaces of Mn_3O_4 nanoparticles were also negatively charged. In this situation, there is no absorption occurrence on the surface of Mn_3O_4 nanoparticles (upper part of Scheme 2). When the pH value of solution is lower than the IEPs, the Mn_3O_4 nanoparticles with positively charged surfaces can rapidly adsorb PCP molecules due to easily formation of more active sites on the fresh and clean surfaces of Mn_3O_4 nanoparticles (lower part of Scheme 2). The desorption performance of PCP was also investigated. When the colloidal sample with PCP completely absorbed was ultrasonically treated for 5 min, approximately 50% of the PCP can be desorbed as determined from the UV−vis absorption spectrum (dash line in Figure 5a). It is known that the precursor complexes can be first formed when the organic compounds are absorbed at the active sites, which would then be decomposed into Mn^{2+} and radicals. These radicals could be further oxidized or coupled,[40,41] which will lead to the red shift of absorption spectra of PCP desorbed from Mn_3O_4 nanoparticles as reflected in Figure 5a. Our preliminary experiments demonstrated that the as-prepared pure Mn_3O_4 nanoparticles can effectively and expediently remove trace levels of PCP from aqueous solution. The underlying physicochemical mechanisms for PCP removal are desirable for further study using as-synthesized pure Mn_3O_4 nanoparticles with clean and fresh surfaces.

Conclusions

In summary, we demonstrated a new methodology for preparing ultrafine Mn_3O_4 nanocrystals by laser ablation of an Mn target in deionized water without addition of other chemical reagents. The particles are tetragonal Mn_3O_4 phase and show a size in the range of 7.1−9.2 nm. A plausible formation process for manganese oxide nanoparticles is proposed based on the rapid reactive quenching between laser-generated manganese species and water molecules. The tetragonal Mn_3O_4 exhibits well ferromagnetic and paramagnetic performance at low and room temperature, respectively. Interestingly, the as-prepared Mn_3O_4 nanoparticles display good performance in trace and rapid removal of PCP in aqueous solution.

Acknowledgment. This work was financially supported by the National Natural Science Foundation of China (Grant

No.10974204, 50931002), the Hundred Talent Program of the Chinese Academy of Sciences, and the President Foundation from Hefei Institutes of Physical Science.

References and Notes

(1) Piligkos, S.; Rajaraman, G.; Soler, M.; Kirchner, N.; Van Slageren, J.; Bircher, R.; Parsons, S.; Gudel, H. U.; Kortus, J.; Wernsdorfer, W.; Christou, G.; Brechin, E. K. *J. Am. Chem. Soc.* **2005**, *127*, 5572.

(2) Yoshikai, N.; Zhang, S. L.; Yamagata, K. I.; Tsuji, H.; Nakamura, E. *J. Am. Chem. Soc.* **2009**, *131*, 4099.

(3) Reddy, A. L. M.; Shaijumon, M. M.; Gowda, S. R.; Ajayan, P. M. *Nano Lett.* **2009**, *9*, 1002.

(4) Armstrong, A. R.; Bruce, P. G. *Nature* **1996**, *381*, 499.

(5) Kuratani, K.; Tatsumi, K.; Kuriyama, N. *Cryst. Growth Des.* **2007**, *7*, 1375.

(6) Shen, Y. F.; Zerger, R. P.; DeGuzman, R. N.; Suib, S. L.; McCurdy, L.; Potter, D. I.; O'Young, C. L. *Science* **1993**, *260*, 511.

(7) Kolts, J. H.; Delzer, G. A. *Science* **1986**, *232*, 744.

(8) Wang, W. M.; Yang, Y. N.; Zhang, J. Y. *Appl. Catal., A* **1995**, *133*, 81.

(9) Baldi, M.; Finocchio, E.; Milella, F.; Busca, G. *Appl. Catal., B* **1998**, *16*, 43.

(10) Li, X. Q.; Zhou, L. P.; Gao, J.; Miao, H.; Zhang, H.; Xu, J. *Powder Technol.* **2009**, *190*, 324.

(11) Zhang, L. C.; Zhou, Q.; Liu, Z. H.; Hou, X. D.; Li, Y. B.; Lv, Y. *Chem. Mater.* **2009**, *21*, 5066.

(12) Drofenik, M.; Zcaron; nidaršič, A.; Kristl, M.; Košak, A.; Makovec, D. *J. Mater. Sci.* **2003**, *38*, 3063.

(13) Ramachandran, R. *J. Mater. Sci.: Mater. Electron.* **2002**, *13*, 257.

(14) Ching, S.; Roark, J. L.; Duan, N.; Suib, S. L. *Chem. Mater.* **1997**, *9*, 750.

(15) Seo, W. S.; Jo, H. H.; Lee, K.; Kim, B.; Oh, S. J.; Park, J. T. *Angew. Chem., Int. Ed.* **2004**, *43*, 1115.

(16) Ozkaya, T.; Baykal, A.; Kavas, H.; Köseoglu, Y.; Toprak, M. S. *Physica B* **2008**, *403*, 3760.

(17) Mafune, F.; Kohno, J. Y.; Takeda, Y.; Kondow, T.; Sawabe, H. *J. Phys. Chem. B* **2001**, *105*, 5114.

(18) Tsuji, T.; Iryo, K.; Watanabe, N.; Tsuji, M. *Appl. Surf. Sci.* **2002**, *202*, 80.

(19) Link, S.; Burda, C.; Nikoobakht, B.; El-Sayed, M. A. *J. Phys. Chem. B* **2000**, *104*, 6152.

(20) Yang, G. W. *Prog. Mater Sci.* **2007**, *52*, 648.

(21) Liang, C. H.; Shimizu, Y.; Masuda, M.; Sasaki, T.; Koshizaki, N. *Chem. Mater.* **2004**, *16*, 963.

(22) Liang, C. H.; Shimizu, Y.; Sasaki, T.; Koshizaki, N. *J. Phys. Chem. B* **2003**, *107*, 9220.

(23) Yeh, M. S.; Yang, Y. S.; Lee, Y. P.; Lee, H. F.; Yeh, Y. H.; Yeh, C. S. *J. Phys. Chem. B* **1999**, *103*, 851.

(24) Zeng, H. B.; Cai, W. P.; Li, Y.; Hu, J. L.; Liu, P. S. *J. Phys. Chem. B* **2005**, *109*, 18260.

(25) Zeng, H. B.; Li, Z. G.; Cai, W. P.; Cao, B. Q.; Liu, P. S.; Yang, S. K. *J. Phys. Chem. B* **2007**, *111*, 14311.

(26) Liang, C. H.; Sasaki, T.; Shimizu, Y.; Koshizaki, N. *Chem. Phys. Lett.* **2004**, *389*, 58.

(27) Qin, W. J.; Kulinich, S. A.; Yang, X. B.; Sun, J.; Du, X. W. *J. Appl. Phys.* **2009**, *106*, 114318.

(28) Ledoux, G.; Amans, D.; Dujardin, C.; Masenelli-V, K. *Nanotechnology* **2009**, *20*, 445605.

(29) Yang, S. G.; Fu, H. B.; Sun, C.; Gao, Z. Q. *J. Hazard. Mater.* **2009**, *161*, 1281.

(30) Schueller, B. S.; Yang, R. T. *Ind. Eng. Chem. Res.* **2001**, *40*, 4912.

(31) Lepoint, T.; Mullie, F. *Ultrason. Sonochem.* **1994**, *1*, S13.

(32) Suslick, K. S.; Casadonte, D. J.; Green, M. L. H.; Thompson, M. E. *Ultrasonics* **1987**, *25*, 56.

(33) Lu, W. G.; Liu, Q. S.; Sun, Z. Y.; He, J. B.; Ezeolu, C.; Fang, J. Y. *J. Am. Chem. Soc.* **2008**, *130*, 6983.

(34) Zhang, L. H.; Wu, J. J.; Liao, H. B.; Hou, Y. L.; Gao, S. *Chem. Commun.* **2009**, 4378.

(35) Liu, Q. X.; Wang, C. X.; Yang, G. W. *Phys. Rev. B* **2005**, *71*, 155422.

(36) Sakka, T.; Iwanaga, S.; Ogata, Y. H.; Matsunawa, A.; Takemoto, T. *J. Chem. Phys.* **2000**, *112*, 8645.

(37) Wang, W. Z.; Xu, C. K.; Wang, G. H.; Liu, Y. K.; Zheng, C. L. *Adv. Mater.* **2002**, *14*, 837.

(38) Jiao, F.; Harrison, A.; Hill, A. H.; Bruce, P. G. *Adv. Mater.* **2007**, *19*, 4063.

(39) Petrie, R. A.; Grossl, P. R.; Sims, R. C. *Environ. Sci. Technol.* **2002**, *36*, 3744.

(40) Stone, A. T. *Environ. Sci. Technol.* **1987**, *21*, 979.

(41) Laha, S.; Luthy, R. G. *Environ. Sci. Technol.* **1990**, *24*, 363.

JP104510A